Structural Analysis of the APT Superconducting Cavities*

M. Cola, G. Ellis, R. Gentzlinger, R. Mitchell#, LANL, Los Alamos, NM

Abstract

The Accelerator Production of Tritium (APT) high-energy linac utilizes superconducting radio-frequency (SCRF) niobium cavities that are enclosed within titanium helium vessels. The vessels are filled with liquid helium that floods the cavities and maintains the 2 K operating temperature. Analyses consist of design calculations for all critical cavity assembly components, cavity tuning sensitivity analysis, active tuner and bench tuner load determination, cavity assembly cool-down analysis, natural frequency and random response analyses, inertia friction weld analysis, and critical flaw size calculations. The design calculations used the *ASME Boiler and Pressure Vessel Code* as a guide where applicable to ensure a successful design. This paper will present the results of the various analyses and point out areas requiring more work.

1 INTRODUCTION

The cavity assembly design has gone through a number of iterations over the last four years [1] before the design described in this paper was finalized. The most significant change to the cavity was to increase the five-degree slope of the β=0.64 cavity wall to a ten-degree slope. Analysis showed that this modification made it possible to eliminate stiffeners between the cells, reducing the fabrication cost significantly.

The second major design change dealt with the outer helium vessel. The original configuration had a tear-drop shape, with flat bulkheads. The tuner-end bulkhead had a flexure integrally machined into it to provide for tuning compliance. Detailed stress analyses showed that this design was not acceptable without stiffeners on the flat bulkheads, as well as on the relatively flat sides between the bulkheads. Increasing the tuning range eventually led to the demise of this design in favor of the vessel within a vessel approach. Two cylindrical vessels are used to house and contain the liquid helium around the cavity (Fig. 1). The inner vessel supplies support for the cavity and tuner while providing stiffness to the large, outer cylinder. The outer cylinder provides the required storage volume for the liquid helium. Welded bellows between the cavity and inner vessel provide tuning compliance, in addition to assembly and cool-down tolerances.

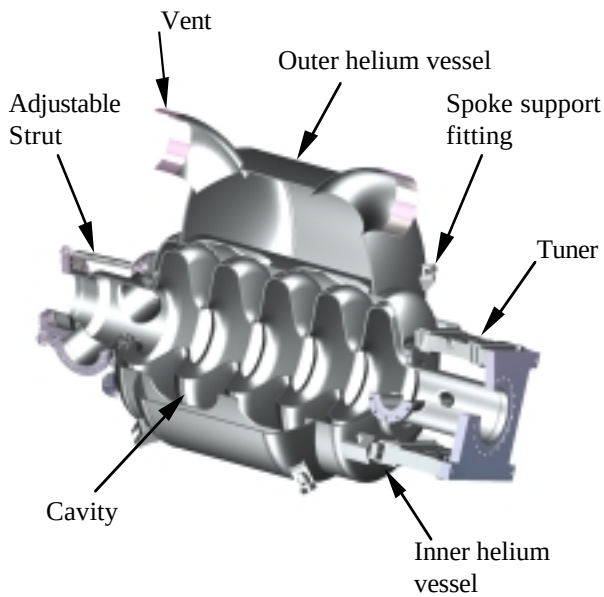

Figure 1. The current β=0.64 cavity and helium vessel.

2 OPERATING ENVIRONMENTS

The cavity is assembled at room temperature and then cooled to 2.15 K in a superfluid helium bath. As the cool gas and liquid enter through the vent pipe at the top of the helium vessel, localized cooling occurs for components directly in line with the coolant flow. The localized cooling results in thermal and stress gradients. During the cool-down process, pressures up to 2.2 atm can build up external to the cavity, but internal to the helium vessel. Since this occurs during the cool-down process, the components are assumed to be at room temperature. Once the assembly is at its operating temperature of 2 K, a fault condition can lead to boil-off pressures reaching 3 atm. For this condition, the components are assumed to be at 2 K. Superimposed on these pressures is the tuning deflection of ±0.04 in. from nominal for the 5-cell cavity. During leak checking at room temperature, a pressure of 1 atm external to the helium vessel exists.

Plant vibration is also a concern. Pumps and other sources can transmit vibrations through the floor, plumbing, and other hardware into the cavity assembly to producing unwanted cavity vibrations.

* Work supported by the Department of Energy under contract No. DE-AC04-96AL89607.
# E-mail:rrm@lanl.gov

3 CAVITY ASSEMBLY DESIGN CALCULATIONS

3.1 Design Allowables

The design calculations used design allowables based on the *ASME Boiler and Pressure Vessel Code*, Section III, where possible. In cases where the code would be overly conservative, other criteria were used, as will be described later. The design allowables used were:

Design allowable stress, S_m:

$$S_m = \text{the lesser of } 2/3\ \sigma_y \text{ or } 1/3\ \sigma_{ult};$$

Primary membrane stress intensity, P_m, must be less than or equal to the design allowable:

$$P_m \le S_m;$$

Primary membrane, P_m, plus bending stress, P_b, must be less than or equal to 1.5 times the design allowable:

$$P_m + P_b \le 1.5\ S_m; \text{ and}$$

Primary, P_m and P_b, plus secondary stress, Q, must be less than or equal to 3 times the design allowable:

$$P_m + P_b + Q \le 3\ S_m.$$

3.2 Material Properties

The structural components of the APT cavity assembly consist of pure niobium (RRR=250 and RRR=40) and pure titanium (Grade 2). Welds between Nb (RRR=250) and Nb (RRR=250), Nb (RRR=40) and Nb (RRR=40), Ti and Ti, Nb (RRR=250) and Nb (RRR=40), and Nb (RRR=40) and Ti are present in the assembly. A comprehensive material testing program [2] was initiated to determine mechanical properties for the base and welded materials at 295 K, 77 K, and 4.2 K. The properties shown in Table 1 were used in the actual design calculations and represent the minimum values obtained from material specifications and the testing program. In an effort to simplify and to remain conservative, the minimum numbers represent the minimum that could be determined from looking at base metal and weld metal information. In other words, a distinction was not made between weld and parent material properties.

Table 1. Minimum material properties used for design calculations.

Material	Young's Modulus (Mpsi)	Min. Yield Strength (ksi)	Min. Tensile Strength (kai)	Min. Elongation (%)	Design Allowable (ksi)
Nb (295 K)	14.2	7.0	21.0	40.0	4.7
Nb (4 K)	14.2	45.0	45.0	1.0	15.0
Ti (295 K)	16.8	40.0	50.0	27.0	16.7
Ti (4 K)	16.8	120.5	162.0	18.0	54.0

3.3 β=0.64 Cavity Design Calculations

3.3.1 Cavity Model Description

The original configuration for the β=0.64 cavity utilized a five-degree wall slope to maximize performance and still allow the chemicals to drain from the cavity after polishing. The shallow wall slope required the cavity to have external support [3] to avoid collapse. The support structure was difficult and expensive to build. In an effort to eliminate the support structure, a ten-degree wall slope was analyzed. The steeper slope reduced the performance slightly (~4%), but it improved the structural performance. Analyses determined the safe nominal wall thickness for the cavity to be 4 mm (0.157 in.). The model used for this calculation was an axisymmetric, second-order, ABAQUS 5.7 finite element model as shown in Fig. 2. Solid elements modeled the cavity, while shell elements modeled the bellows. Thinning from chemical etching, forming, and machining weld preps were included in the model geometry. The modeled thickness was 0.148 in. for the nominal thickness; 0.133 in. for the thinned iris region; and 0.103 in. for the weld prepped equator region.

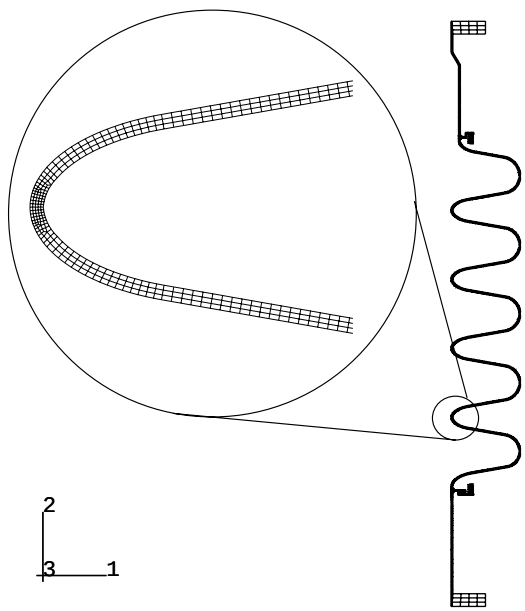

Figure 2. Axisymmetric ABAQUS 5.7 FEM cavity model.

3.3.2 2.2-Atm Cavity Analysis

During cool-down, the cavity may be subjected to a 2.2-atm external pressure while still near room temperature. In addition, the tuner could be at its deflection limit. Analyses looked at the maximum stress intensities for the cavity loaded at 2.2 atm and compressed and extended

0.04 in. The material was assumed to be linear elastic. Results were:

$$P_m = 5500 > S_m = 4700 \text{ psi}$$

$$P_m + P_b = 7800 > 1.5\ S_m = 7000 \text{ psi}$$

$$P_m + P_b + Q = 9140 \leq 3\ S_m = 14000 \text{ psi}.$$

The cavity stresses exceed the design allowables for this situation; however, because niobium is a very ductile material at room temperature, it is unlikely that the material will fail prior to collapse.

A plastic collapse analysis was performed on the cavity to determine the collapse pressure. The niobium included work hardening based on data obtained from MST-6 at LANL (curve DDL3-2148V) [4] as shown in Fig. 3.

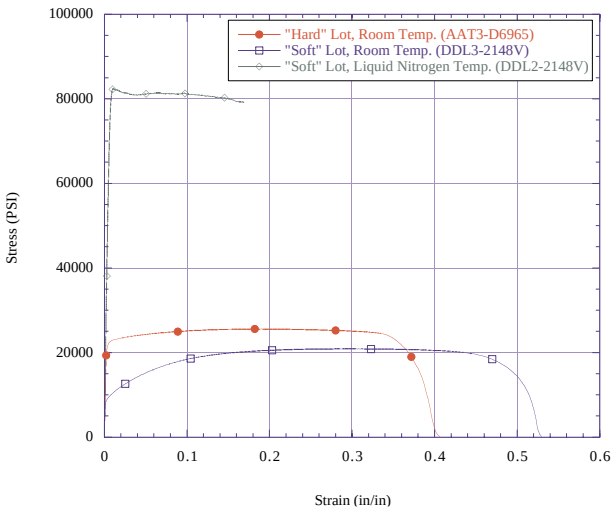

Figure 3. Material property curves for Nb (RRR=250).

A plot of pressure versus equivalent plastic strain for the iris and equator regions is shown in Fig. 4. Significant collapse occurs between 5 and 6 atm and is completely collapsed at 7.7 atm. Figures 5 and 6 show plastic strain contours and the deformed cavity shape at 5.9 and 7.7 atm, respectively. The 2.2-atm pressure load is at least a factor of 2 below the collapse pressure. In addition to remaining below the collapse pressure, the maximum strain should be below its failure strain. At 5.9 atm, the plastic strain is only 2.7%, well below its minimum elongation of 40%. Even at 7.7 atm when the cavity has completely collapsed, the plastic strain is 21.2%, about half its failure strain.

In addition to ensuring its structural adequacy at 2.2 atm, the cavity should also remain functional after receiving the pressure load. Since the cavity does develop small plastic strains, there is some detuning that takes place. To determine the amount of detuning, the cavity was pressurized to 2 and 3 atm and then the pressure was removed, leaving the plastically deformed geometry. The amount of frequency shift was determined to be 23.23 and 180.34 kHz [5], corresponding to a tuning displacement of 73 and 565 µm (0.0029 and 0.022 in.) for the 2- and 3-atm pressure, respectively. Since the tuner operating range is ±1016 µm (0.040 in.), the 2-atm pressure presents no real problem for the tuner. Even the 3-atm pressure, might be absorbed by the tuner depending on its nominal position.

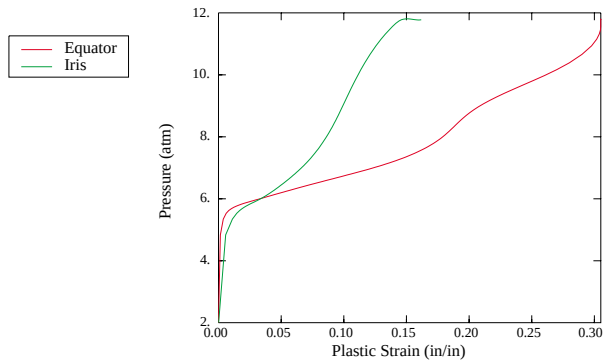

Figure 4. Plot of pressure (atm) vs. equivalent plastic strain (in./in.) for the equator and iris.

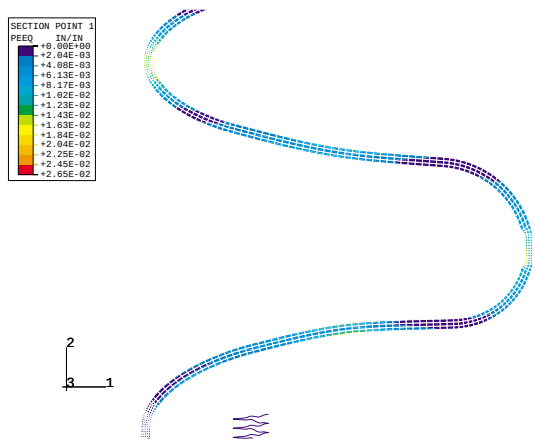

Figure 5. Maximum equivalent plastic strain of 2.7% at 5.9 atm.

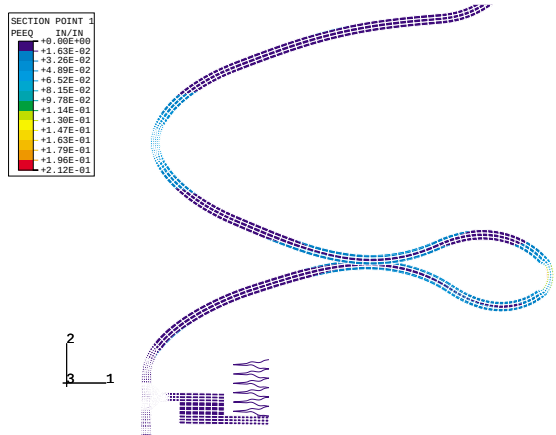

Figure 6. Maximum equivalent plastic strain of 21.2% at 7.7 atm.

3.3.3 3.0-Atm Cavity Analysis

Next, the cavity was subjected to the 3-atm external pressure, in addition to the tuning deflections, while at its 2 K operating temperature. The axisymmetric model shown in Fig. 2 was used for this calculation and assumed elastic material properties. Results were:

$$P_m = 7900 \leq S_m = 15000 \text{ psi}$$

$$P_m + P_b = 10600 \leq 1.5\ S_m = 22500 \text{ psi}$$

$$P_m + P_b + Q = 12000 \leq 3\ S_m = 45000 \text{ psi}.$$

All stress intensities were well below the design allowable values.

3.3.4 1.0-Atm Coupler Tube Analysis

During operation of the cavity, there is a 1-atm pressure differential acting on the coupler tube toward the cavity. An ABAQUS 3-D first-order shell model of the entire cavity (Fig. 7) was used to calculate the stress in the coupler tube to the beam tube joint. The maximum von Mises stress was found to be 3500 psi (Fig. 8), and is less than the design allowable, S_m, of 4700 psi.

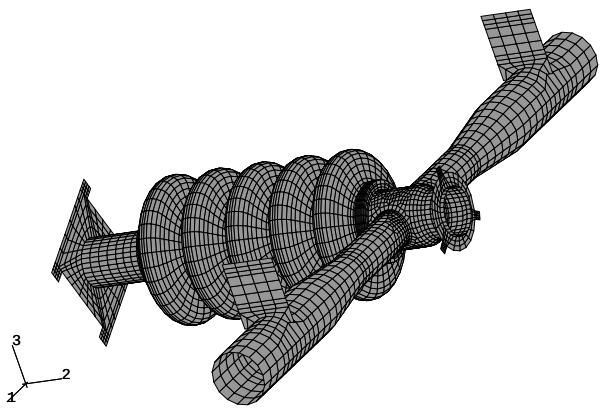

Figure 7. ABAQUS FEM model of the cavity assembly used to calculate the coupler tube stress.

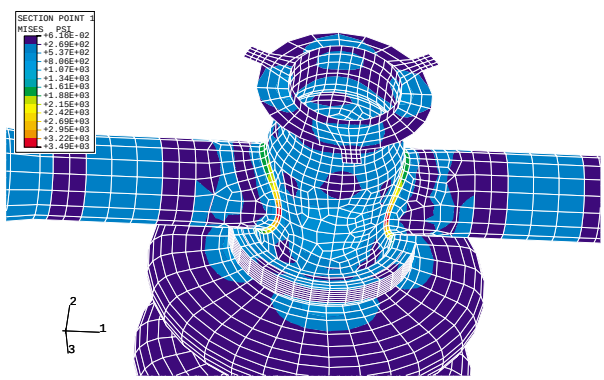

Figure 8. Contour plot of von Mises stress caused by coupler tube load.

3.4 Helium Vessel Design Calculations

The helium vessel is constructed of pure, unalloyed Grade 2 titanium. The initial design scheme was to employ a tear-drop shaped vessel to house the cavity. This configuration was driven primarily by the cryogenics requirements. Many design calculations were performed on this basic concept to try to make it acceptable from a structural standpoint, but it became apparent that various stiffeners would be required, and still the design was marginal. A new configuration (Fig. 1) was eventually adopted. This design met the cryogenic concerns, and resulted in a very robust helium vessel.

A full 3-D ABAQUS 5.7 FEM model was developed for the helium vessel (Fig. 9). The model used second-order shell elements to model the vessel with thicknesses of 1/4 in. and 3/16 in. for the vessel bulkheads and sides, respectively. Elastic material properties were used.

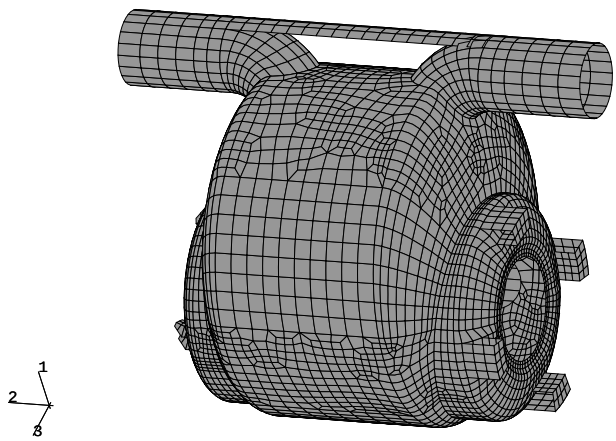

Figure 9. ABAQUS FEM model of the helium vessel.

The model was subjected to (1) a 1-atm external pressure at room temperature; (2) a 2.2-atm internal pressure at room temperature; and (3) a 3-atm internal pressure at 2 K. A contour plot of von Mises stress is shown in Fig. 10 for the 3-atm internal pressure case. The results were:

1-atm external pressure at room temperature:
maximum von Mises stress = 4430 ≤ S_m = 16700 psi;

2.2-atm internal pressure at room temperature:
maximum von Mises stress = 9800 ≤ S_m = 16700 psi; and

3-atm internal pressure at 4 K:
maximum von Mises stress = 13300 ≤ S_m = 54000 psi.

All stresses are below the design allowables.

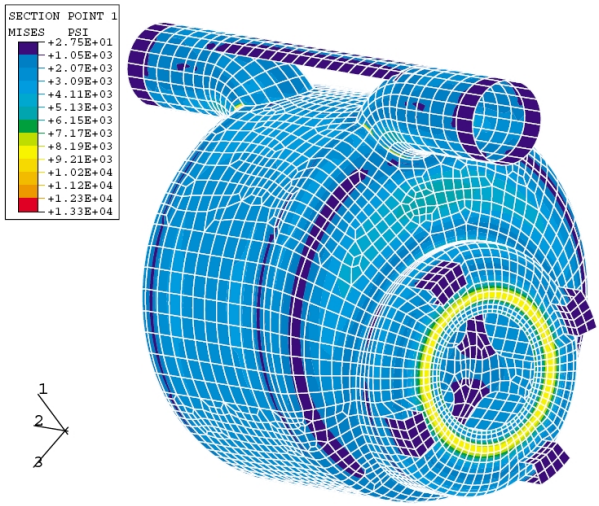

Figure 10. von Mises stress contours for a 3-atm internal pressure on the helium vessel.

3.5 Helium Vessel Spoke Bracket Calculations

The spoke brackets are welded to the outer helium vessel's bulkhead as shown in Fig. 1. The spokes are initially tensioned to 400 lb and run from the helium vessel to the vacuum vessel, suspending the helium vessel within the cryomodule. As the helium vessel is cooled, the vessel shrinks, pulling the spokes tight. Belleville washers at the warm ends of the spokes take up some of the thermal strain, but the spokes are tensioned to 2400 lb after cool-down is complete. An ABAQUS model was developed to simulate a quarter of the outer helium vessel with second-order shell elements, and to simulate the support bracket with second-order solid elements. The inner helium vessel was not modeled. Because the inner helium vessel tends to restrain the outer helium vessel, the outer vessel nodes were fixed in both displacement and rotation where the outer helium vessel is welded to the inner vessel.

The initial configuration had a bracket leg thickness of 0.08 in. and a length of 2.28 in. For this configuration, localized von Mises stresses of approximately 102000 and 32200 psi were developed in the bracket and the outer vessel, respectively, as shown in Fig. 11. Since these stresses are developed at 4 K, brittle fracture was a concern. To reduce the stress, the bracket leg thickness was increased to 0.12 in. and the length was increased to 4.5 in. This configuration reduced the maximum stress in the bracket down to 20000 psi, below the 54000 psi design allowable.

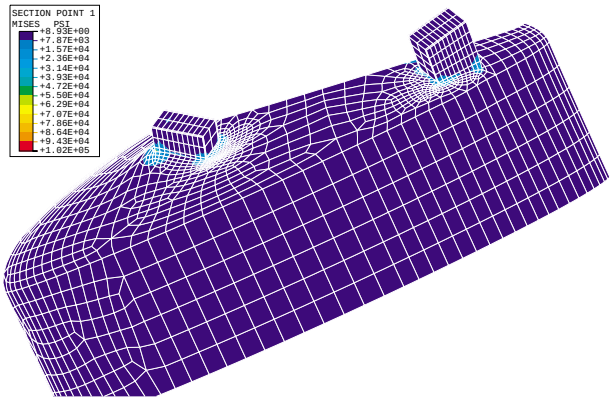

Figure 11. von Mises stress contour plot of the spoke bracket and outer helium vessel.

3.6 Weld Residual Stress

The welds in the cavity and the helium vessel cannot be stress relieved; as a result, residual welding stress will be present. To account for the residual stress in the design allowable calculations, the residual stress was superimposed on the stress calculations just discussed. The residual stress was considered a secondary stress and assumed to be at the yield stress level of the material. For conservatism, the residual stress was assumed to be in the same direction as the operating stress, and the results are shown below.

For the cavity at 3 atm (2 K):

$(P_m + P_b + Q)_{operational}$ = 12000 psi
$(P_m + P_b + Q)_{residual}$ = 7000 psi
$(P_m + P_b + Q)_{operational} + (P_m + P_b + Q)_{residual}$
= 19000 psi ≤ 45000 psi.

For the cavity at 2.2 atm (295 K), the design allowables are exceeded as discussed earlier. In this case, the plastic strains are well below the failure strain, so the residual stress will not lead to failure.

For the coupler tube at 1 atm (295 K):

$(P_m + P_b + Q)_{operational}$ = 3500 psi
$(P_m + P_b + Q)_{residual}$ = 7000 psi
$(P_m + P_b + Q)_{operational} + (P_m + P_b + Q)_{residual}$
= 10500 psi ≤ 14000 psi.

For the helium vessel at 3 atm (2 K):

$(P_m + P_b + Q)_{operational}$ = 13300 psi
$(P_m + P_b + Q)_{residual}$ = 40000 psi
$(P_m + P_b + Q)_{operational} + (P_m + P_b + Q)_{residual}$
= 53300 psi ≤ 162000 psi.

For the helium vessel at 2.2 atm (295 K):

$(P_m + P_b + Q)_{operational}$ = 9800 psi
$(P_m + P_b + Q)_{residual}$ = 40000 psi
$(P_m + P_b + Q)_{operational} + (P_m + P_b + Q)_{residual}$
= 49800 psi ≤ 50000 psi.

For the helium vessel at 1atm (295 K):

$(P_m + P_b + Q)_{operational}$ = 4430 psi
$(P_m + P_b + Q)_{residual}$ = 40000 psi
$(P_m + P_b + Q)_{operational} + (P_m + P_b + Q)_{residual}$ = 44430 psi ≤ 50000 psi.

For the spoke bracket at 3 atm (2 K):

$(P_m + P_b + Q)_{operational}$ = 20000 psi
$(P_m + P_b + Q)_{residual}$ = 40000 psi
$(P_m + P_b + Q)_{operational} + (P_m + P_b + Q)_{residual}$ = 60000 psi ≤ 162000 psi.

3.7 Design Calculation Summary

To determine the adequacy of the cavity and helium vessel design, stresses were compared to design allowables. For all load cases, the stresses were below the allowable values except for the cavity subjected to a 2.2-atm pressure at room temperature. For this case, a more detailed analysis using work hardened material properties was carried out to determine the collapse pressure as well as the plastic strain at the point of collapse, and the amount of cavity detuning. The 2.2-atm pressure is more than a factor of 2 below the collapse pressure, and the plastic strains are more than a factor of 10 below the failure strain. In addition, the amount of tuning required to maintain the correct cavity radio-frequency is well within the tuner's displacement range. From a stress analysis standpoint, the design of the cavity and helium vessel is acceptable.

4 CAVITY ASSEMBLY COOL-DOWN ANALYSIS

4.1 Cool-Down Model Description

As the cavity is cooled down from room temperature, the assembly is subjected to thermal stress gradients, as well as various mechanical loads. A full 3-D ABAQUS 5.7 model (Fig. 12) was developed to simulate the initial cooling scenario, as well as the final cooled-down state at 2 K. Note that this model is similar to other models cited in this paper. For this particular simulation the beam tube and vent pipe on the coupler side of the cavity were lengthened to the centerline of a cavity pair. Symmetry boundary conditions were placed on the ends of the tubes to simulate a rigid connection between the two cavities within a cryomodule. The spokes were modeled with beam elements and were pre-tensioned to 400 lb. The coefficients of thermal expansion that were used from 295 to 2 K were 2.724×10^{-6}, 2.948×10^{-6}, and 5.77×10^{-6}/°F (4.903×10^{-6}, 5.306×10^{-6}, and 10.39×10^{-6}/K) for niobium, titanium, and stainless steel, respectively. The spokes were assigned a value of 3.7×10^{-6}/°F (6.66×10^{-6}/K) to simulate the effect of a temperature variation along their length and to provide a 2400 lb preload at the steady-state operating temperature.

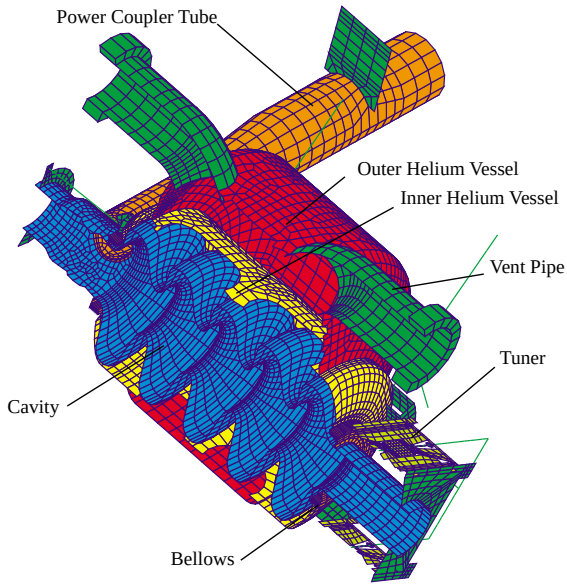

Figure 12. Cutaway of full 3D cavity assembly model.

4.2 Transient Cool-Down Results

To simulate the transient cooling of the assembly, the inlet vent pipe (in this case, the coupler-side pipe) was cooled to 2 K, while the rest of the vessel remained at 295 K. The 2.2-atm pressure internal to the helium vessel but external to the cavity and the 1-atm coupler tube load were also included. Fig. 13 shows the undeformed and deformed (magnified 100 times) geometry for the transient case without the pressures applied. The transient case tends to drop the end of the beam tube at the coupler tube by 0.011 in., while lifting the tuner end by 0.012 in. This places the coupler tube in bending as shown in the stress contour plot (without the pressure loading) in Fig. 14. The maximum stress in the cavity without pressure loading is 3530 psi, well below the design allowable. The maximum stress in the helium vessel is 21100 psi localized in the strut mount and vent pipe to helium vessel weld region. The stress is within the peak stress design allowable. Fig. 15 plots the stress with the pressure loading included. For this scenario, the stress in the coupler tube increased to 6400 psi, but remained lower than the iris region. The helium vessel stress increased slightly to 22100 psi as seen in the stress contours of Fig. 16.

The spokes also see the effect of the helium vessel movement. The analysis pre-tensioned the spokes to approximately 450 lb, slightly more than the specified 400 lb. When the vent pipe is cooled, the coupler end of the vessel drops, tightening the upper spokes and loosening the lower spokes. The opposite occurs at the opposite end (where the vessel lifts), loosening the upper spokes and tensioning the lower spokes. The analysis

predicts that the tensioned spoke's load will increase to approximately 1120 lb, while the loosened spokes near the coupler tube will actually go into compression by approximately –210 lb. The tension of the loosened spokes at the tuner side drops to about 100 lb. It is important to note that the analysis does not take into account any Belleville washers. The washers may add compliance to the system and tend to allow the cavity to dip even further. Additionally, the spokes most likely will not take compressive loads, so that may cause the cavity to drop slightly more since the model predicted two spokes to go into slight compression.

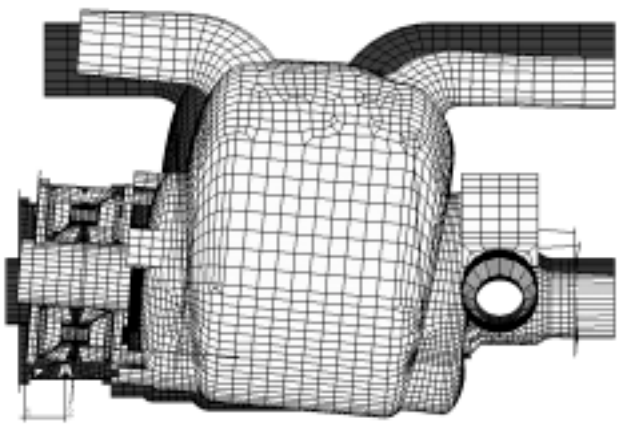

Figure 13. Displaced geometry for transient cool-down (displacements magnified 100 times).

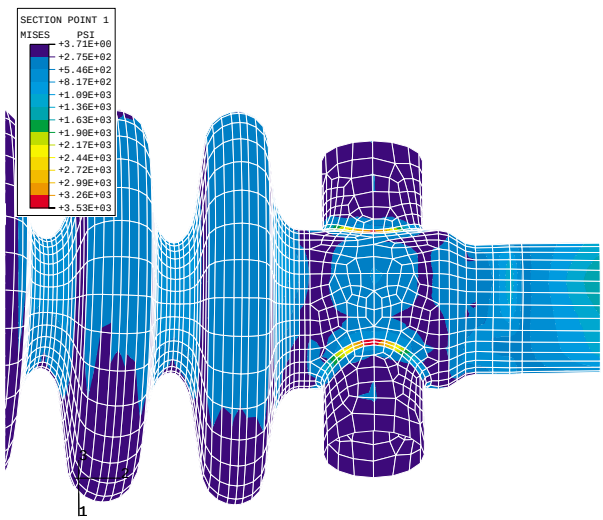

Figure 14. von Mises stress in the coupler tube area during transient cool-down without pressure load.

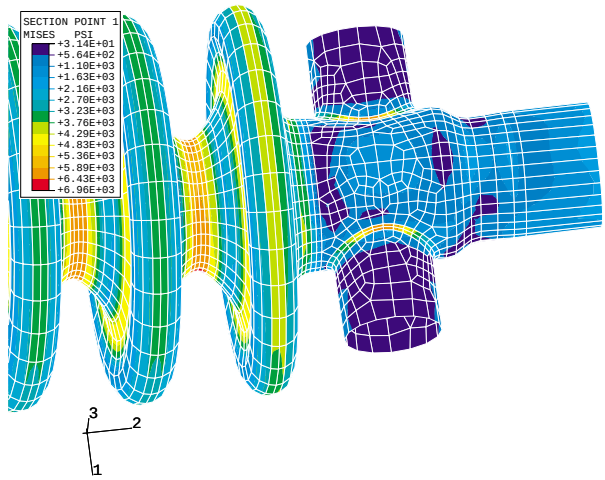

Figure 15. von Mises stress in the coupler tube area during transient cool-down with pressure load.

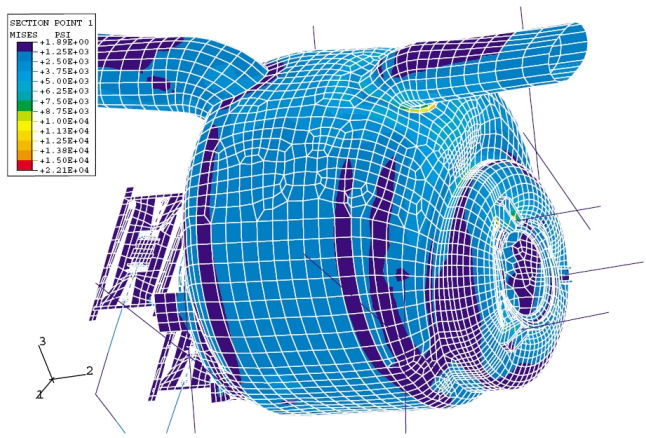

Figure 16. von Mises stress in the helium vessel during transient cool-down with pressure load.

4.3 Steady-State Results

The model used in the transient case was also used for the steady-state case, but the components were allowed to cool to the 2 K operating temperature. The 1-atm coupler tube load remained, but the 2.2-atm pressure was increased to 3 atm. The deformed and undeformed geometries without pressure loading are shown in Fig. 17, where the deformations are magnified 100 times. Notice that the assembly has leveled out to within about 0.002 in., but the coupler port on the beam tube is moved toward the symmetry plane by 0.012 in. The stress contours (without the pressure loading) in the coupler tube area are shown in Fig. 18. The maximum stress (not including where the stainless steel flanges compress the niobium) in the cavity without pressure loading is 3200 psi, well below the design allowable. The maximum stress in the helium vessel is 33900 psi in the tuner flange area as seen in Figs. 17 and 20. The high stress is a result of the

titanium tuner being rigidly bolted to the stainless steel flange. As a result of this analysis, the tuner mounting flange was modified to account for the dissimilar thermal expansion of the two materials. The stresses in the remainder of the helium vessel are below 5000 psi.

The pressure loads were then included, and the results for the stresses in the coupler tube area are shown in Fig. 19. For this scenario, the stress in the coupler tube increased to 5500 psi but remained lower than the iris region. Aside from the tuner region, the helium vessel stress increased from below 5000 psi to 15000 psi, as seen in the stress contours of Fig. 20.

The contraction of the helium vessel caused the spokes to tighten to between 2980 and 3320 lb. This is slightly higher than the specified 2400 lb load.

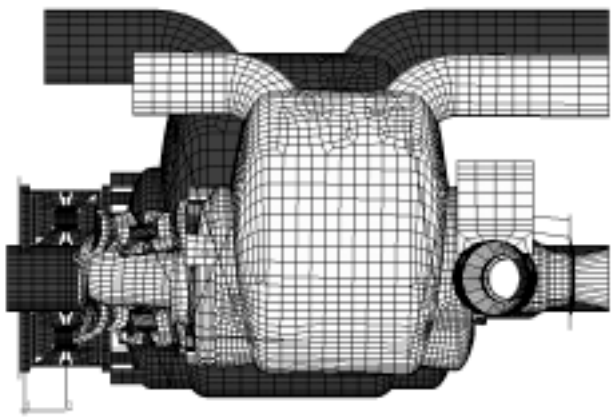

Figure 17. Displaced geometry for steady-state cool-down (displacements magnified 100 times).

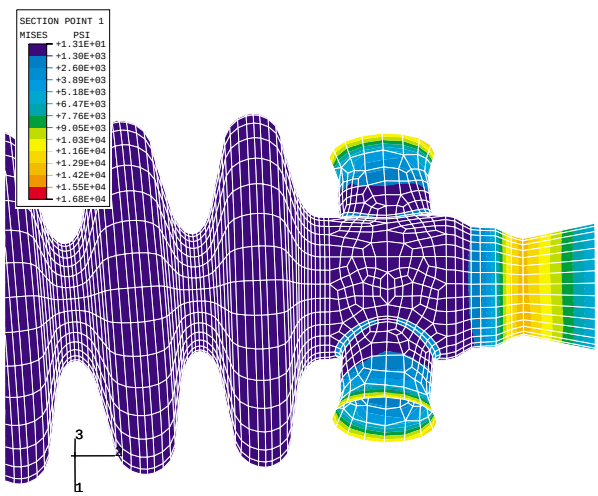

Figure 18. von Mises stress of the coupler tube area after reaching operating temperature, without the pressure load.

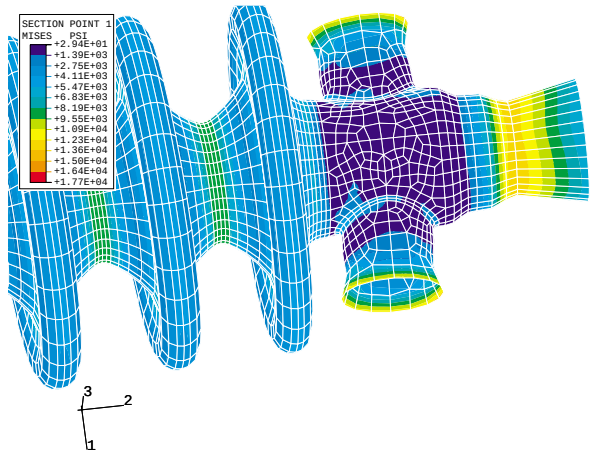

Figure 19. von Mises stress of the coupler tube area after reaching operating temperature, with the pressure load.

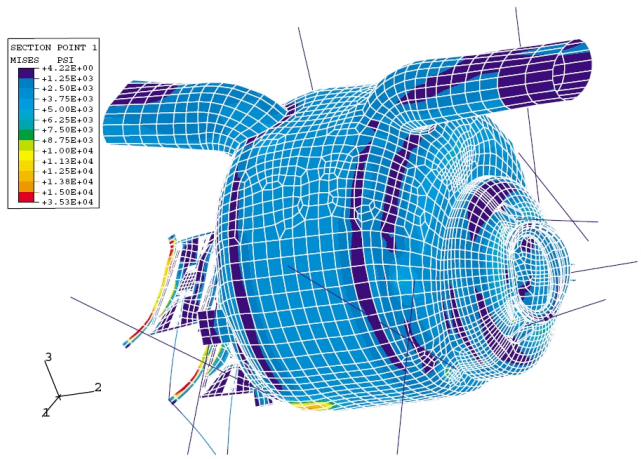

Figure 20. von Mises stress in the helium vessel after reaching operating temperature, with pressure load.

4.4 Localized Cooling

In addition to the generalized cooling stresses discussed above, localized stresses are generated as cool gas and liquid dump onto a small area of the cavity and helium vessel. To determine a conservative localized stress, the surface of a few elements in contact with the helium were set at 2 K for both the helium vessel and cavity. The opposite surface and the remainder of the elements were kept at 295 K. A linear temperature profile was assumed through the thickness of the cooled elements. The maximum principal stresses were determined to be 17400 psi for the cavity and 20900 psi for the helium vessel. Even with conservatism, these stresses remain below the design allowable values.

4.5 Assembly Cool-Down Results Summary

Two cool-down scenarios were analyzed in addition to the localized cooling calculation. When the entire assembly was cooled to operating temperature, relatively large stresses developed between the titanium tuner and the stainless steel flange. As a result, the tuner mount was redesigned to account for the thermal expansion differences between the two parts. Other stresses remained below their design allowable values.

During the transient cool-down scenario, the coupler end of the cavity dropped by 0.011 in. and the tuner end lifted by 0.012 in. Also, a pair of spokes saw a 200 lb compressive force as the cavity dipped. When the entire assembly was cooled to its steady-state temperature, the ends of the cavity leveled off to within 0.002 in., but the coupler port on the beam tube was moved toward the symmetry plane by 0.012 in.

5 CRITICAL FLAW SIZE CALCULATION

The previous calculations dealt with eliminating the possibility of a ductile failure. Here, the same analyses will be used to determine a critical flaw size to ensure that brittle fracture does not occur. Brittle failure occurs when a tensile stress near a crack tip is large enough to drive the crack. For brittle fracture, all stresses in a given orientation must be superimposed. A few things that make the assembly susceptible to brittle fracture are welds that are not stress relieved, cold forming operations that are not stress relieved, and the brittle nature of niobium at 4 K. In general, the operating stresses are fairly low, which reduces the likelihood of brittle fracture. The lack of published fracture toughness data for niobium and Grade 2 titanium, led to a comprehensive fracture toughness testing program [2].

5.1 Determine Maximum Stress

To determine a critical flaw size, the maximum stress in the worst-case orientation must be determined. This can be a very complicated calculation due to the many different ways that stresses are generated in the structures. For the assembly, the primary sources of stress are from pressures, displacements, thermal strains, and residual stresses. A conservative approach assumes that all maximum stresses act in the same orientation and, thus, take the sum of all the various stresses. If the critical flaw size turns out to be a reasonable size that can be detected without too much difficulty and cost, then there is no reason to refine the calculations.

The critical area in the cavity is in the iris weld at 2 K. Stress contributions are from the 3-atm pressure and 0.04 in. tuner displacement (12000 psi), weld residual stress (7000 psi), and localized cooling (17400 psi). Stress from the general cool-down is negligible, and welding should eliminate the forming stress. The sum of the various stresses is 36400 psi in the cavity.

A similar calculation is performed for the helium vessel where the critical area occurs at the vent pipe to helium vessel weld. Stress contributions are from the 3-atm pressure and general cool-down (15000 psi), weld residual stress (40000 psi), and local cooling (20900 psi). The sum of the various stresses is 75900 psi in the helium vessel.

5.2 Determine Fracture Toughness Requirements

To determine the required fracture toughness for the applied stress, a hand calculation for a single-edge-notched specimen was performed [6]:

$$K_I = \sigma\sqrt{\pi a}\, f\left(\frac{a}{b}\right)$$

where:

K_I is the stress - intensity factor,

σ is the tensile stress,

a is the crack length, and

b is the thickness.

A plot of the stress-intensity factor as a function of crack length can be determined as shown in Fig. 21 for the cavity and helium vessel.

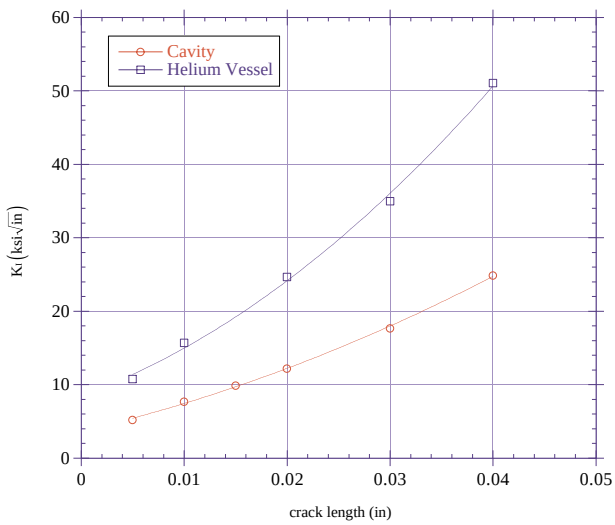

Figure 21. Calculated stress-intensity factors for the cavity and helium vessel.

5.3 Determine Critical Flaw Size

As mentioned earlier, a test program was initiated [2] to determine the Mode I fracture toughness for niobium, titanium, and the various weld combinations used in the cavity assembly. The minimum Mode I fracture toughness values obtained for either the base material or weld are 58 and 21 ksi$\sqrt{\text{in}}$. for titanium and niobium, respectively.

The corresponding crack lengths are 0.034 in. for niobium and 0.044 in. for titanium obtained from Fig. 21. The actual maximum flaw size used for part acceptance is 0.016 in. for niobium and 0.018 in. for titanium. These flaw sizes assure a safety factor of at least 2 while maintaining a realistically detectable flaw size without great expense. It is important to remember that the calculations to determine the maximum tensile strength are conservative , which tends to increase the safety factor.

6 NATURAL FREQUENCY AND RANDOM RESPONSE ANALYSES

Mechanical vibrations of the cavity tend to affect the shape of the cavity cells, shifting the radio-frequency of the cavity from its ideal tuned frequency during operation. Because the allowable RF frequency shift might be as low as ±100 Hz, which corresponds to a longitudinal deflection of only 12.4×10^{-6} in., knowledge of the cavity response is important. The amount of acceptable lateral deflection is unknown at this time due to the difficulty posed by the three-dimensional nature of the calculation. To determine the lateral sensitivity, a test to relate frequency to lateral deflection is needed.

A modal survey testing program is underway [7] to determine natural frequencies and mode shapes of the β=0.64 5-cell cavity. This data can help validate the finite element models that can be used to predict the response of the entire cavity assembly. At this time, a detailed model of the cavity assembly has been created and subjected to floor vibration, but the model has not yet been validated with test data. Figure 12 shows a cutaway of the model and is similar to the model described in the cool-down calculations. The model includes the cavity and helium vessel suspended from pre-tensioned spokes and power coupler flexures. The active tuners and the tuning arms are simulated. The model assumes there are bellows in the vent pipe and beam tube on both sides of the cavity. The input power spectral density (PSD) is input into the end of the spokes and at the power coupler flexures. The vacuum vessel was not included in the model, but it could affect the results greatly.

One major difficulty in performing a random response analysis is determining the proper input PSD to use for the calculation. Since the APT structure is not built, it is impossible to know precisely what PSD to use. Here at LANL, a program was developed previously to determine the floor vibration for the Ground Test Accelerator (GTA) program. The facility contains many pumps and miscellaneous hardware that may be analogous to the APT project. The input PSD used for the preliminary calculations presented here represents a bounded PSD, as measured for GTA, with a 6-db gain and is shown in Fig. 22 [8]. The 6-db gain increases the total rms displacement by a factor of two over the measured data. Notice that the majority of the excitation occurs between 20 and 30 Hz, corresponding to the common rotational velocity of the majority of the pumps used in the facility. Other potential sources such as pumps mounted very near the cavity were not considered at this time.

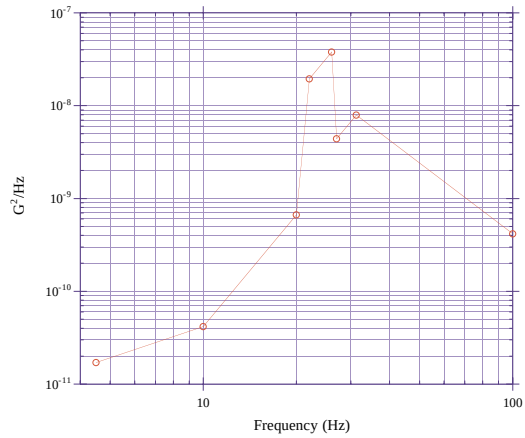

Figure 22. Input PSD used in the calculation.

6.1 Natural Frequencies and Mode Shapes

Before performing a random response analysis, the natural frequencies and mode shapes are determined for the cavity assembly. Based on the input PSD from Fig. 22, the natural frequencies between 20 and 60 Hz are those most likely to be excited. Table 2 lists the first ten natural frequencies.

Table 2: Cavity assembly natural frequencies.

Mode	Natural Frequency (Hz)
1	13.9
2	34.2
3	45.5
4	46.7
5	54.0
6	64.0
7	71.0
8	79.2
9	86.0
10	101.0

The first three mode shapes are shown in Figs. 23-25. The first mode (13.9 Hz) is essentially a longitudinal mode in which the cavity is moving as an assembly, causing the coupler tubes to bend. The natural frequency of this mode is governed primarily by the weight of the cavity assembly, the stiffness of the power couplers, and to a lesser degree the stiffness and tension in the spokes. The second mode (34.2 Hz) is the first lateral mode (Fig. 24). The cavity is essentially flexing laterally,

causing the power coupler tubes to move side to side. The cavity stiffness is the main contributor to this mode. The third mode (45.5 Hz), is the first vertical mode (Fig. 25). The cavity is being flexed vertically, similar to Mode 2. However, the power couplers provide more vertical support than lateral support, so the frequency is slightly higher for the vertical mode than for the lateral mode.

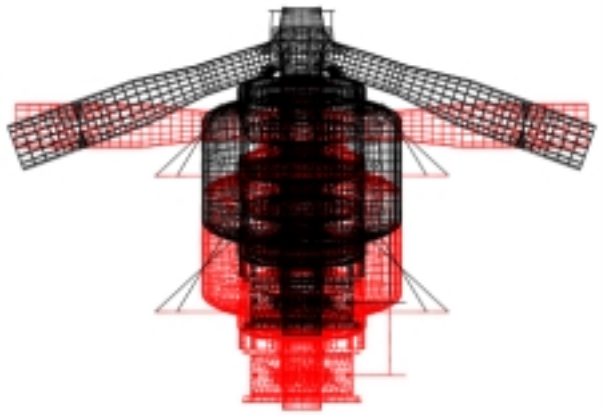

Figure 23. First mode (13.9 Hz) is a longitudinal mode.

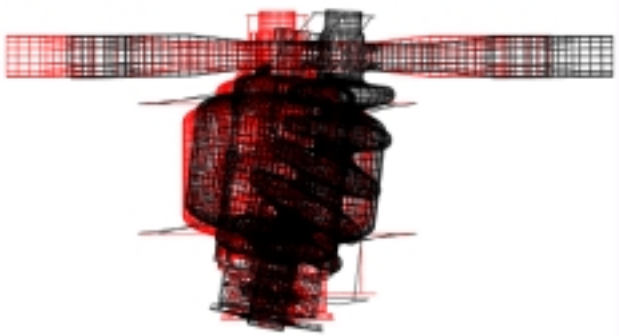

Figure 24. Second mode (34.2 Hz) is the first lateral mode.

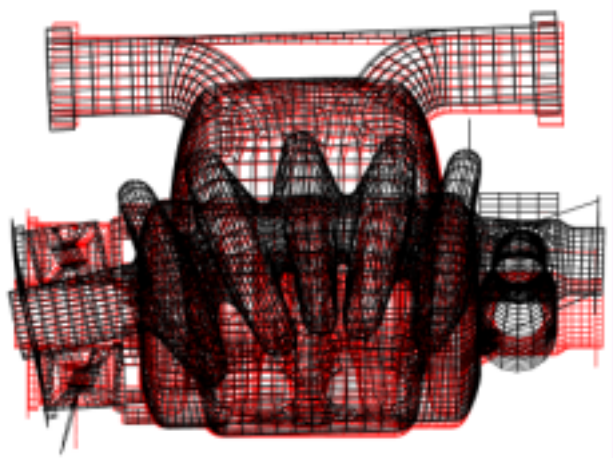

Figure 25. Third mode (45.5Hz) is the first vertical mode.

6.2 Random Response Analysis

A random response analysis of the cavity assembly was performed using the PSD shown in Fig. 22, having a total rms displacement of 7.7 x 10^{-6} in. The excitation was placed on the fixed ends of the spokes and power coupler flexures. The cavity assembly was excited in all three directions, and the response of the cavity was determined between various nodes of the cavity. The relative rms displacement was determined between the two beam tubes and between the coupler beam tube and the middle cell in all three directions. A global model damping of 1% was assumed.

For longitudinal excitation, the relative rms displacements are plotted in Fig. 26. The maximum rms deflection of 1.74 x 10^{-6} in. is generated in the longitudinal direction between the coupler tube and the middle cell. The rms deflections in the off-axis directions are approximately 1 x 10^{-6} in. or less. The majority of the cavity deflection occurs at 13.9 Hz, which corresponds to the first longitudinal mode (Fig. 23).

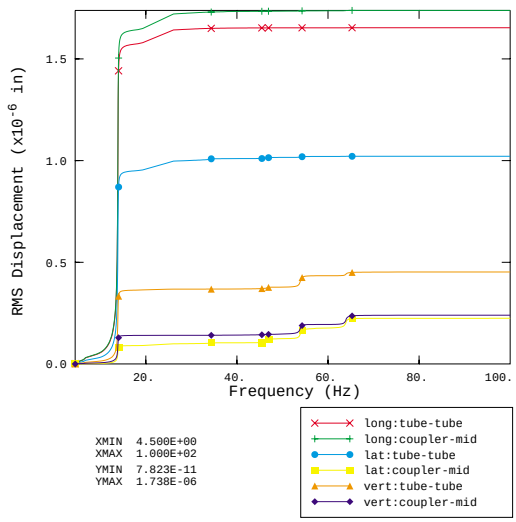

Figure 26. Total rms displacement vs. frequency for a longitudinal excitation.

For a lateral excitation, the relative rms displacements are plotted in Fig. 27. The maximum rms deflection of 51.7 x 10^{-6} in. is generated in the lateral direction between the two beam tubes. The rms deflections in the off-axis directions are approximately 12.0 x 10^{-6} in. in the vertical direction, and 3.73 x 10^{-6} in. in the longitudinal direction. We suspect that much of the longitudinal deflections are the result of the cavity being bent, thus causing the nodes on the surface of the cavity to move relative to each other in the longitudinal direction. A better approach would be to measure the distance along the centerline between two areas of the cavity. The majority of the cavity deflection occurs at 34.2 Hz, which corresponds to the first lateral mode as shown in Fig. 24. The second increase in deflection occurs at 46.7 Hz, which corresponds to Mode 4, the second predominately lateral mode.

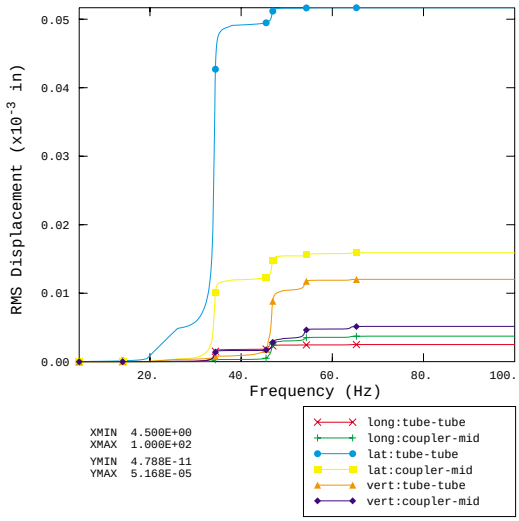

Figure 27. Total rms displacement vs. frequency for a lateral excitation.

For a vertical excitation, the relative rms displacements are plotted in Fig. 28. The maximum rms deflection of 16.1 x 10^{-6} in. is generated in the vertical direction between the two beam tubes. The rms deflections in the off-axis directions are approximately 7.57 x 10^{-6} in. in the lateral direction, and 5.28 x 10^{-6} in. in the longitudinal direction. Again, much of the longitudinal deflections are the result of the cavity being bent, thus causing the nodes on the surface of the cavity to move relative to each other in the longitudinal direction. A better approach would be to measure the distance along the centerline between two areas of the cavity. The majority of the cavity deflection occurs at 45.5 Hz, which corresponds to the first vertical mode as shown in Fig. 25. The second increase in deflection occurs at 54.0 Hz, which corresponds to Mode 5.

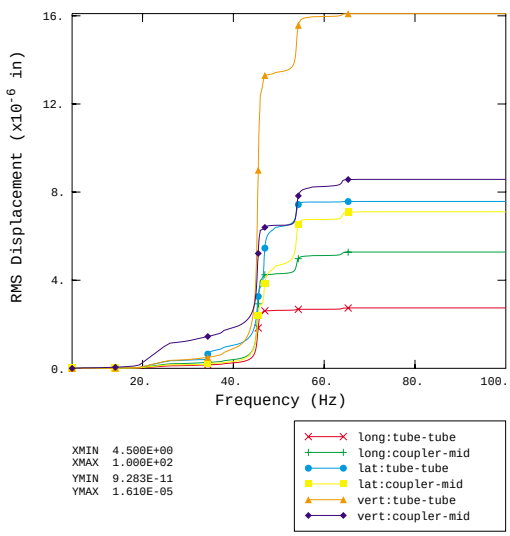

Figure 28. Total rms displacement vs. frequency for a vertical excitation.

6.3 Random Response Summary

An input PSD was used to excite the cavity in the longitudinal, lateral, and vertical directions to determine the relative total cavity rms displacements. It is important to remember that the model has not been validated with test data and that the vacuum vessel was not included. The total rms displacement of the input PSD was 7.7 x 10^{-6} in. The total rms cavity deformations were 1.74 x 10^{-6}, 51.7 x 10^{-6}, and 16.1 x 10^{-6} in. for longitudinal, lateral, and vertical directions. To relate rms displacements into peak displacements, the rms value is often multiplied by a factor of 3 to give a probability that 99.7% of the time the amplitude will be below this value, assuming a Gaussian distribution. Because many random phenomena approach a Gaussian distribution [9], this approach produces a reasonable value for the peak deflection. As mentioned earlier, we would like to keep the cavity longitudinal deformation to be less than 12.4x10^{-6} in. for a 5-cell cavity, or 6.2x10^{-6} in. for half a cavity. The maximum calculated displacement for half the cavity is 3(1.74x10^{-6}) or 5.22x10^{-6} in., which is within the requirement. The requirement for the lateral and vertical directions is not known at this time, but a similar technique could be followed.

The vacuum vessel and its structure can greatly affect the cavity response and should be included in the analysis. If the deformations are deemed too large, the vacuum vessel could be redesigned to reduce the cavity displacements. The vacuum vessel can be designed to help isolate the cavity from floor vibrations by having its natural frequency less than about half the natural frequency of the cavity mode you are trying to suppress. Of course a poorly designed vacuum vessel could increase the cavity deformations. The effect of nearby pumps should also be determined.

7 INERTIA FRICTION WELD ANALYSIS

7.1 Weld Description

The titanium vent line in the helium vessel must transition into a stainless steel line within the cryomodule. The engineering design and development (ED&D) cavity assembly also has instrumentation ports that must transition from stainless steel to titanium. In an effort to eliminate braze joints within the cryogenic plumbing system, a program was initiated to develop an inertia friction (IFR) weld between stainless steel and titanium tubing [10]. The process of IFR welding involves a rotating part that is driven into a stationary part to form a weld joint between the two parts. Weld parameters include rotational speed, axial force, and flywheel moment of inertia. IFR welding is inherently solid-state and exhibits a rapid thermal cycle that restricts base-metal interdiffusion. The initial weld development

focused on 1.0-in. diameter tubes with a 0.08-in. wall thickness. To aid in the IFR weld development, a FEM model was developed for the joint and compared to burst and tensile testing at room temperature. The required room-temperature joint strength is a minimum 40 ksi nominal stress, and if the joint fails, it should show ductile features.

7.2 1-in. Diameter Tube Weld

The problem associated with welding titanium to stainless steel is that brittle intermetallics are formed at the interface, producing a very brittle joint. To produce a usable joint, various interlayers were tried that might be compatible with both titanium and stainless steel. The interlayer found to produce the best performance was pure niobium. To produce the joint, the stainless steel tube is first welded to the niobium interlayer; then the titanium tube is welded to the niobium/stainless steel tube. Before welding, the outside diameters of all three materials were the same, but the niobium's inner diameter was smaller than the stainless steel or titanium. As the stainless steel and niobium were forced together, material disruption occurred which caused the stainless steel to deform. This disruption led to the nominal weld shape shown in the micrograph (Fig. 29).

O.D.

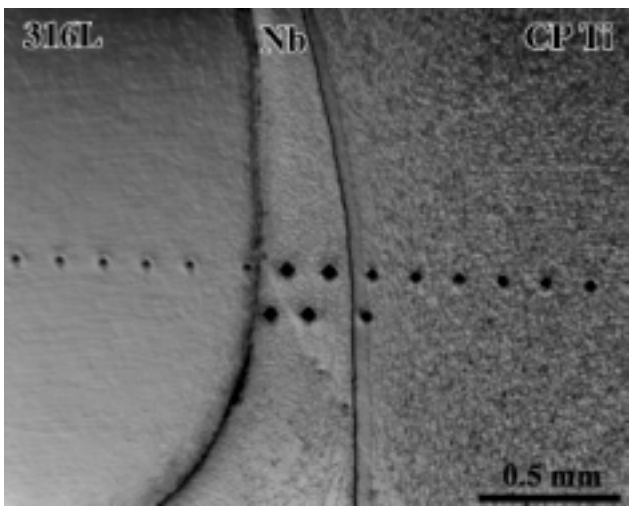

I.D.

Figure 29. Section through the wall of a 1-inch diameter IFR welded tube. Note the upset in the stainless steel at the inner diameter. This micrograph also shows microhardness indentations.

7.3 IFR Weld FEM Model

To aid the weld development, a finite element model was developed for various joint geometries. The baseline geometry (Fig. 30) simulates the nominal 1.0-in. diameter tube configuration as shown in Fig. 29. The niobium layer thickness varied from approximately 0.007 in. at the outside diameter, to 0.013 in. at the center, to 0.027 in. at the inside diameter. To numerically study the effect of niobium layer geometry on joint strength, three additional models were developed. The first assumed a flat niobium layer of 0.0075 in. thick (Fig. 31). The second assumed a flat niobium layer of 0.013 in thick (Fig. 32). The third assumed a U-shaped niobium layer, where the niobium layer was 0.027 in. at the inside and outside diameters, and 0.013 in. at the center (Fig. 33). The flat niobium layers could be produced by machining off a portion of the outside and inside diameters after welding. The U-shaped weld assumed that the inner and outer diameters of the niobium protruded beyond the surfaces of the stainless steel and titanium tubes. When the weld is generated, the stainless steel will be disrupted on both the inside and outside diameters.

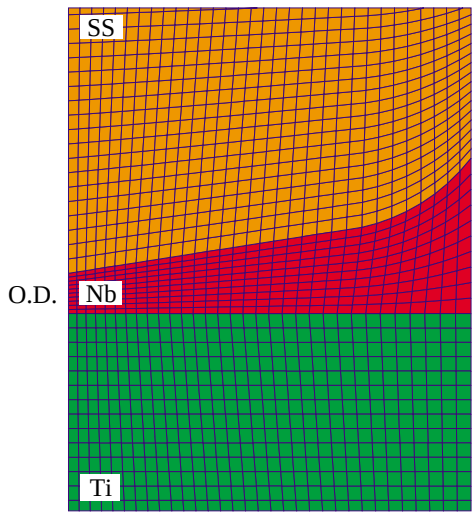

Figure 30. Weld region of the IFR weld model with the baseline niobium interlayer.

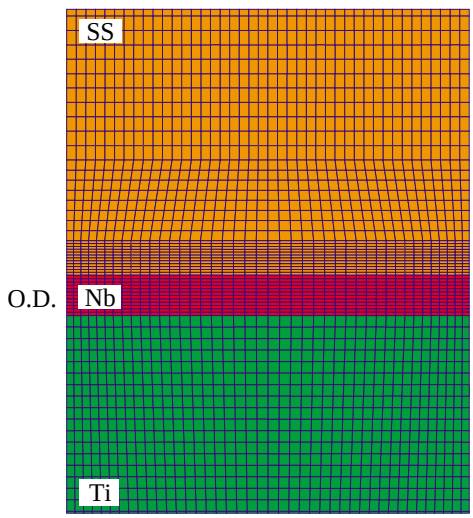

Figure 31. Weld region of the IFR weld model with a 0.0075 in. flat niobium interlayer.

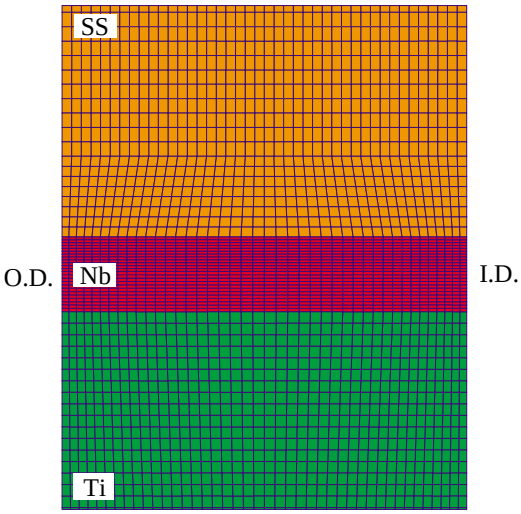

Figure 32. Weld region of the IFR weld model with a 0.013 in. flat niobium interlayer.

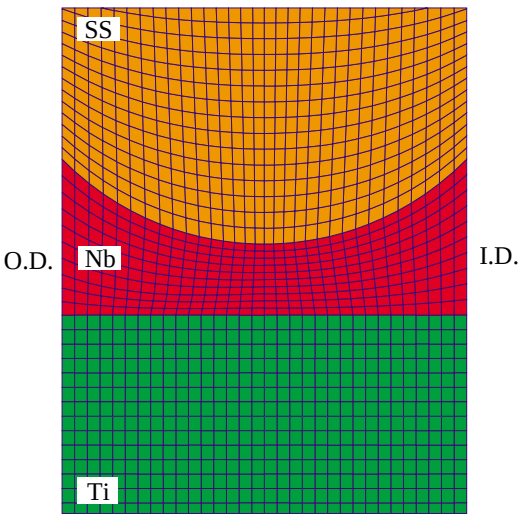

Figure 33. Weld region of the IFR weld model with a U-shaped niobium interlayer.

All FEM analyses were ABAQUS axisymmetric models. The models included residual hoop stress from joining dissimilar materials at elevated temperatures. To generate the residual stress, nodes near the weld were cooled down from 1500°F to 70°F. The models also accounted for the increase in hardness of the titanium and stainless steel near the weld zone (Fig. 34). The increased hardness is due to cold working effects as the joint was formed, and it tends to increase the yield strength. To account for the increased hardness, the initial portion of the stress-strain curves for the titanium and stainless steel were lopped off, increasing the yield strength in proportion to the increase in hardness.

The models simulated a burst test and a tensile test at room temperature. The burst model was a static analysis, while the tensile test model was a dynamic quasi-static analysis. The quasi-static analysis allowed the calculation to run to part failure in a reasonable amount of time.

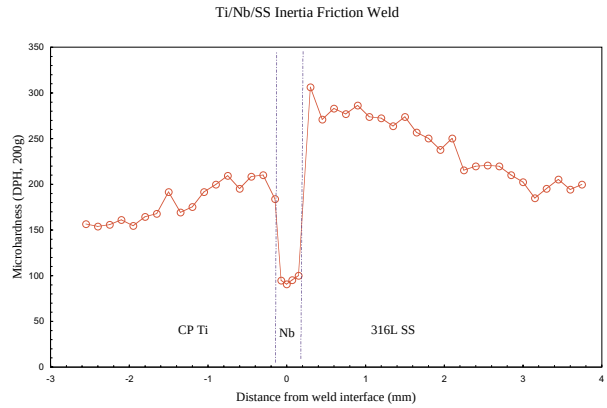

Figure 34. Microhardness of an IFR welded joint.

7.4 IFR Weld Results

7.4.1 Burst Results

Burst tests at room temperature were performed on welded specimens to determine the failure mechanism and burst strength [11]. One specimen failed through the weld, but it was determined that most of the niobium was extruded out of the weld, which led to a weak joint. The second specimen failed in the titanium. The maximum pressure achieved was 10160 psi. It was observed that the weld region acted as a constraint. Both the titanium and stainless steel tubing showed significant yielding, but both were restrained at the weld.

Analyses were performed to simulate a burst test on the various weld geometries. As the pressure was ramped up, significant yielding occurred in the bulk titanium material, as well as in the niobium interlayer. From an analysis standpoint, the joint strength was very similar to the titanium strength. All four weld configurations failed between a pressure of 9150 and 9285 psi, approximately 9% lower than the test maximum pressure. The joint geometry had little effect on joint strength. Both testing and analyses showed that the weld region acted to restrain the titanium and stainless steel tubes (Fig. 35). Note that the analysis deformations are magnified five times, but results in qualitatively the same shape as the test specimen. Since material failure tends to be numerically unstable, the analysis was not run out to complete failure, thus limiting the deformations. The restraint at the weld joint is most likely the result of the material cold working near the weld, increasing the yield strength of the titanium and stainless steel.

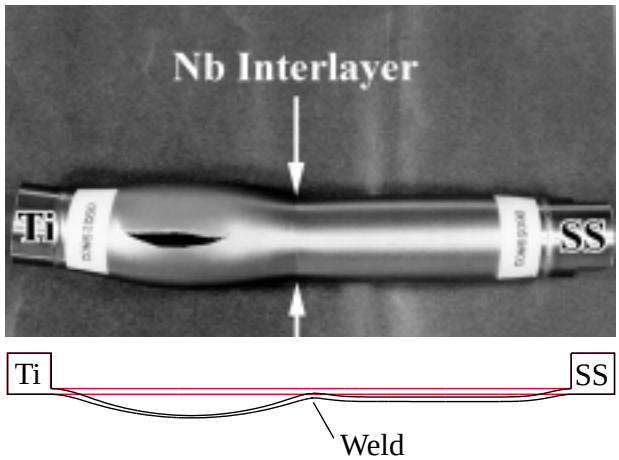

Figure 35. Comparison of the post-burst geometry for the test (top) and analysis (bottom). Note that the analysis deformations are magnified 5 times.

7.4.2 Tensile Results

Tensile tests at room temperature were performed on welded specimens. A specimen having a sound weld would result in failure of the titanium tube away from the weld at a nominal stress of 57.3 ksi, as shown in the micrograph of Fig. 36. The post-test micrograph indicates "necking" in the niobium layer and a shifting of the titanium tube toward the inside diameter as the titanium tube "necked down" prior to failure.

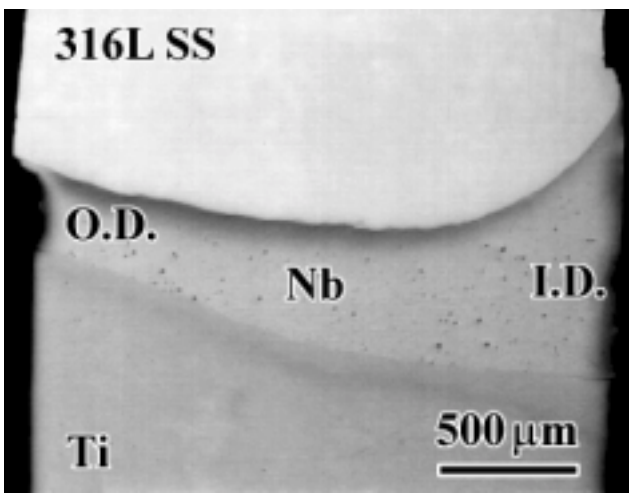

Figure 36. Post tensile test micrograph of a test specimen sectioned through the weld.

Analyses were performed that simulated a tensile test on the four weld configurations. These analyses were quasi-static, dynamic runs to allow the materials to develop significant plastic strains in a reasonable amount of time. All analyses showed that significant plastic strains would be developed in both the titanium and the niobium interlayer, but failure would occur in the niobium, not in the titanium as the test showed. The primary reason for this difference is most likely unknowns in the material properties of the weld region. Fig. 37 shows the deformed geometry and contours of the equivalent plastic strain for the baseline configuration. Failure occurred in the niobium at a nominal stress of 53.4 ksi, which is 7% lower than the tensile test. Note that the niobium layer has significant plastic strains and that "necking" is present in the niobium interlayer as found in the test specimen. The titanium is not shifted toward the inside diameter in this case because the titanium has not "necked down" as in the test specimen. Fig. 38 plots the load versus displacement for all four weld geometries. The flat 0.0075 in. thick niobium configuration produced the strongest joint, while the U-shaped weld produced the weakest. The baseline and 0.013 in. flat niobium configurations produced similar strengths. The minimum nominal joint strength was 49.7 ksi for the U-weld, which is greater than the required strength of 40 ksi. It appears that the niobium layer thickness is the primary reason for the difference in strength. The thinner layers provided more confinement to the niobium, resulting in greater strength. The final niobium interlayer shape does not appear to have as much effect on strength as the layer thickness.

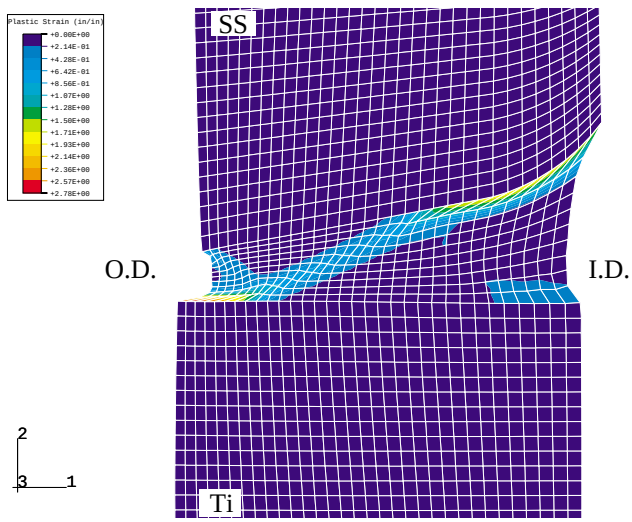

Figure 37. Contour of equivalent plastic strain for the baseline weld configuration.

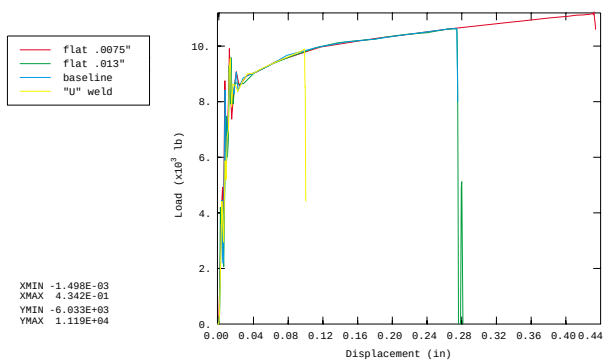

Figure 38. Load-displacement curve for the four weld geometries analyzed.

7.5 IFR Weld Summary

Welds having room-temperature properties superior to titanium were generated. Analyses were unable to predict failure in the titanium tube during tensile loading, but they did predict that the niobium layer can sustain a nominal stress more than twice its bulk ultimate stress. The most likely reason for the lower than tested strength of the weld joint is unknowns in material properties in the weld region. Based on the analysis, the joint geometry is more critical for the tensile load than for the pressure load. All configurations modeled generated greater than 40 ksi nominal joint strength. The niobium layer thickness had more effect on joint strength than the shape of the layer. Larger niobium thickness tends to reduce the niobium confinement, resulting in reduced joint strength. To ensure that the IFR welded joint is acceptable for cryogenic applications, the joints should be tested at 4 K.

8 ACTIVE AND BENCH TUNER LOAD DETERMINATION

8.1 Active Tuner Design Load

To design the active tuner for the cavity, the axial load that the tuner must react must be determined. The maximum load that the tuner would see is the result of the 3-atm pressure being applied to the cavity, in addition to the tuning deflection. The pressure tends to compress the cavity so the tuner must react against that load. Since the cavity has a range of ±0.04 in., the load to deform the cavity must also be included. Axisymmetric models of the β=0.64 and β=0.82 cavities were created to determine the axial reaction force that the tuner must react. The cavities were extended 0.04 in. and a 3-atm pressure was applied while fixing the ends of the cavity. The cavity reaction forces were determined to be 3250 and 3100 lb for the β=0.64 and β=0.82 cavities, respectively. Counteracting this load is the bellows and bellows flange pressure load. The effective area for the bellows is

$$EA = \pi\left(\frac{d_{o_b} + d_{i_b}}{4}\right)^2 - \pi\frac{d_{o_t}^2}{4}.$$

where

d_{o_b} = 8.7 in., the outer diameter of the bellows,

d_{i_b} = 7.7 in., the inner diameter of the bellows, and

d_{o_t} = 6.6 in., the outer diameter of the beam tube.

The effective area of the bellows is then 18.6 in^2, corresponding to an axial force of 820 lb for the 3-atm pressure. The load acting on the tuner is then 2430 lb.

8.2 Bench Tuner Load Calculation

The cavity is constructed by a combination of machining, welding, and metal forming. The fabrication technique produces significant cavity cell tolerances that affect the cavity frequency. Prior to operation, the cavity must be tuned to the correct frequency by plastically deforming the cavity cells until the desired frequency is obtained. Because the cavity must be plastically deformed, significant forces are generated.

Because the β=0.82 cavity is stiffer than the β=0.64 cavity, an axisymmetric model of a β=0.82 mid cell was created using shell elements. The analysis assumed a 0.128 in. (3.26 mm) cavity thickness prior to etching. The iris and equator regions were assumed to be at full thickness for conservatism. The material properties for the base and welded niobium are shown in Fig. 39. The heat affected zones (HAZ) at the iris and equator were assumed to be 1/4 inch long. The material properties were the best estimate of the upper bounds for the weld and base metal based on testing at LANL [4]. The base material yields at 18000 psi, while the HAZ area yields at 8000 psi.

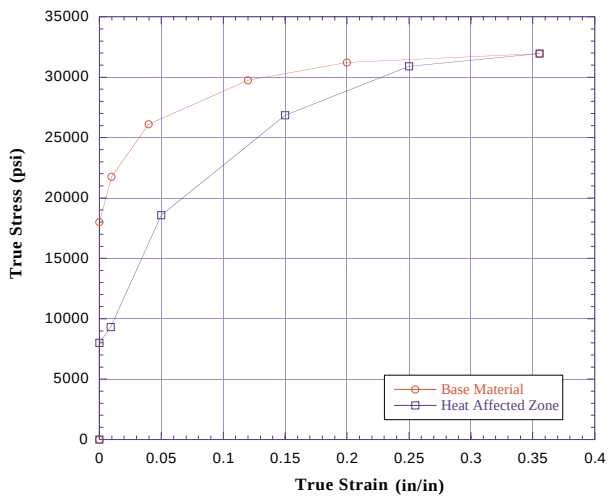

Figure 39. True stress vs. true strain for base niobium and HAZ used in determining the bench tuner load.

To determine the maximum bench tuner load, the cavity was extended or compressed enough to cause yielding and then relaxed. The initial displacement was increased until the permanent deformation was 0.1 in. for a half cell, corresponding to 1 in. for the entire 5-cell cavity. To place the cavity in tension, the nodes at the iris were displaced. To place the cavity in compression, the nodes within the bench tuning plates that make contact with the cavity near the iris were displaced.

The maximum load of 13320 lb occurs when the cavity is placed in tension (Fig. 40). The maximum load in compression is 7930 lb, which corresponds to the plastic buckling load (Fig. 41). The maximum equivalent plastic strain in tension and compression was .016 and .0361 in./in., respectively.

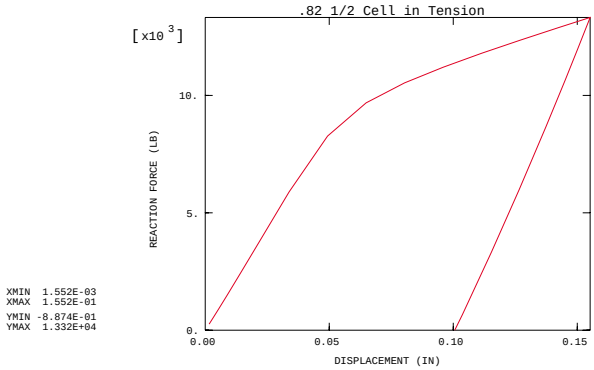

Figure 40. Bench tuning load vs. displacement curve for a β=0.82 1/2-cell cavity in tension.

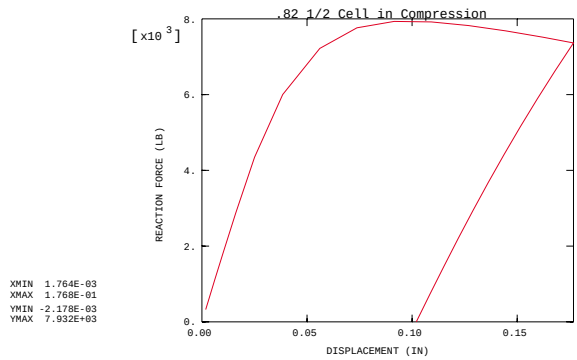

Figure 41. Bench tuning load vs. displacement curve for a β=0.82 1/2-cell cavity in compression.

9 SUMMARY

Analyses consisted of design calculations for all critical cavity assembly components, cavity tuning sensitivity analysis, active tuner and bench tuner load determination, cavity assembly cool-down analysis, natural frequency and random response analyses, inertia friction weld analysis, and critical flaw size calculations. Often times, many design iterations were analyzed numerically before finalizing the design as presented here. As the design evolved, the models were updated where it was thought necessary. The thoroughness of these calculations helped produce a structurally acceptable structure within the time constraints of the project. As the project progresses, more analyses will follow.

10 REFERENCES

[1] R. Gentzlinger et al., "Design, Analysis, and Fabrication of the APT Cavities," for PAC 99, New York City, March 1999.

[2] R. Walsh et al., "Low Temperature Tensile and Fracture Toughness Properties of SCRF Cavity Structural Materials," 9th Workshop on RF Superconductivity, Santa Fe, NM, November 1999.

[3] D. Schrage and E. Swensen, LANL Memo: AOT-1:95-180.

[4] D. Hammon, preliminary data from private conversation, 1998.

[5] F. Krawczyk, private E-mail on frequency shift, 1998.

[6] S. T. Rolfe and J. M. Barsom, "Fracture and Fatigue Control in Structures," Prentice-Hall, Inc., Englewood Cliffs, NJ, 1977.

[7] G. Ellis et al., "Modal Survey of Medium Energy Superconducting Radio Frequency Cavity for Accelerator Production of Tritium Project," 9th Workshop on RF Superconductivity, Santa Fe, NM, Nov. 1999.

[8] T. Butler and S. Ellis, private conversation, 1998.

[9] W.T. Thomson, "Vibration Theory and Applications," Prentice-Hall, Inc., Englewood Cliffs, NJ, 1965.

[10] M.J. Cola et al., "Dissimilar Metal Joints for the APT Superconducting Cavity's Cryogenic Plumbing System," for PAC 99, New York City, March 99.

[11] T. Weeks, "Weld Burst Coupon Test Report," ESA-MT report, April 12, 1999.